Supporting Information

Central metal ion of MOFs modulated fluorescence detection of Fe^{3+}

Haitao Liu,[a] Senlin Li,[a] Bo Zhao,[a] Yanan Gu,[a] Qiaozhen Sun,*[a] Bingguang Zhang*[b]

[a]*School of Materials Science and Engineering, Central South University, Changsha, 410083, China*

[b]*Key Laboratory of Catalysis and Materials Sciences of the State Ethnic Affairs Commission & Ministry of Education, College of Chemistry and Material Science, South-Central University for Nationalities, Wuhan, 430074, China*

*Corresponding author

Email: rosesunqz@csu.edu.cn (Q. Sun)

Email: 3092809@mail.scuec.edu.cn (B. Zhang)

Number of pages: 12

Number of tables: 6

Number of figures: 16

Contents

Section 1 Synthesis of H_2L

The ligand H_2L was synthesized similar to the literature reported.[S1] Step 1: Dimethyl 3',5'-dibromo-[1,1'-biphenyl]-3,5-dicarboxylate (**1**) was purchased from Chemical Book. The precursor **2** was synthesized through the classic Ullmann reaction. Mixing **1** (2.02 g, 5 mmol), imidazole (1.70 g, 25 mmol), L-Proline (0.46 g, 4 mmol), CuI (0.38 g, 2 mmol), K_2CO_3 (2.07 g, 15 mmol) in 150 mL three-necked bottle, and adding 50 mL ultra-dry DMSO into the mixture under nitrogen atmosphere, heating to 125 °C for 48 h, after cooling to room temperature, the crude product was treated by the extraction with water and ethyl acetate. The organic phase with the product was purified by the silica gel column chromatography with the solvent of ethyl acetate/petroleum ether. The white powder of product **2** was obtained. Step 2: Adding **2** (1.15 g, 2.86 mmol) and NaOH (1.14 g, 28.6 mmol) into the mixed solution of THF/MeOH/H_2O (35/35/70 mL), and then heated to 80 °C overnight. After cooling to room temperature, the solvent was evaporated and concentrated hydrochloric acid was added dropwise until the pH value was 6. At last, the product H_2L precipitated. ^{1}HNMR (400 MHz, DMSO): 13.49 (s, 2H), 8.56 (dd, 4H), 8.52 (t, 1H), 8.06 (t, 2H), 8.02 (d, 1H), 7.99 (d, 2H), 7.14 (d, 2H). IR (KBr, cm^{-1}): 3431(vs), 3127(s), 1919(m), 1700 (w), 1609(s), 1550(w), 1502(m), 1403(w), 1317(m), 1228(s), 1132(m), 1093(m), 1064(s), 1013(m), 985(vw), 863(w), 832(w), 756(m), 712(w), 654(w), 607(w), 493(m), 431(vw).

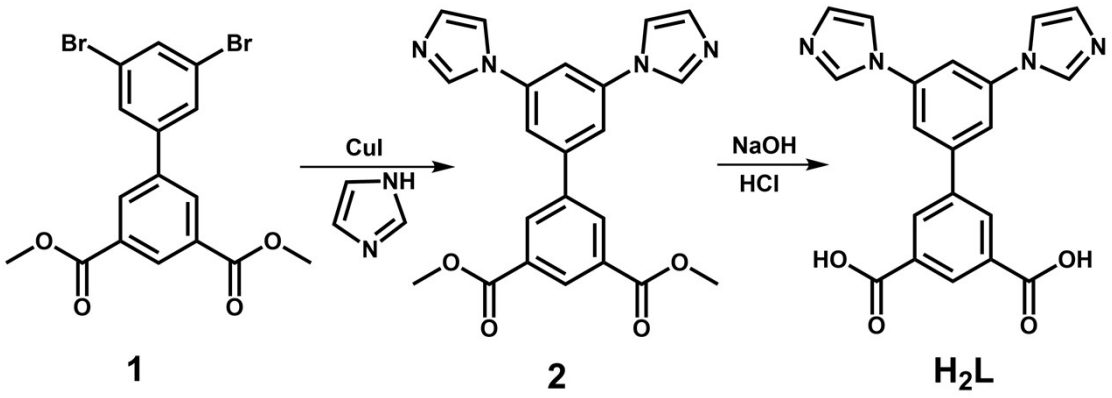

Scheme S1 Synthetic route of H_2L ligand

Section 2 General characterization and structural information

Table S1 Crystal data and structure refinement details for compounds **1** and **2**

Compounds	**1**	**2**
Empirical formula	$C_{20}H_{15}N_4O_{5.5}Zn$	$C_{20}H_{12}N_4O_4Sr$
Formula weight	464.73	459.96
Crystal system	monoclinic	orthorhombic
Space group	*C*2/c	*P*cca
a (Å)	24.585(4)	15.9757(11)
b (Å)	11.4983(18)	12.5349(9)
c (Å)	16.964(5)	8.3633(6)
α (°)	90	90
β (°)	129.258(2)	90
γ (°)	90	90
V (Å^3)	3713.2(13)	1674.8(2)
Z	8	4
D (g/cm^3)	1.663	1.824
Mu (mm^{-1})	1.369	3.259
F(0 0 0)	1896	920
Unique reflections	2754	1542
Observed reflections	4213	1975
R_{int}	0.0622	0.0392
Final *R* indices [$I>2\sigma(I)$]	$R_1 = 0.0498$	$R_1 = 0.0235$
	$wR_1 = 0.1006$	$wR_1 = 0.0533$
R indices (all data)	$R_1 = 0.1018$	$R_1 = 0.0368$
	$wR_2 = 0.1233$	$wR_2 = 0.0567$
Goodness-of-fit on F^2	1.013	1.042

Table S2 Selected Bond Lengths (Å) and Bond Angles (°) for **1** and **2**

1			
Zn(1)-O(1)#1	1.916(3)	Zn(1)-O(3)#2	1.946(3)
Zn(1)-N(3)	1.994(3)	Zn(1)-N(1)#3	2.023(3)
O(1)#1-Zn(1)-O(3)#2	108.76(12)	O(1)#1-Zn(1)-N(3)	119.86(14)
O(3)#2-Zn(1)-N(3)	107.93(13)	O(1)#1-Zn(1)-N(1)#3	105.39(13)
O(3)#2-Zn(1)-N(1)#3	101.86(13)	N(3)-Zn(1)-N(1)#3	111.55(13)
2			
Sr(1)-O(2)#1	2.5380(14)	Sr(1)-O(2)#2	2.5380(14)
Sr(1)-O(2)	2.6241(14)	Sr(1)-O(2)	2.6241(14)
Sr(1)-O(1)	2.6729(14)	Sr(1)-O(1)	2.6729(14)
Sr(1)-N(1)	2.7469(17)	Sr(1)-N(1)	2.7469(17)
O(2)#1-Sr(1)-O(2)#2	73.19(6)	O(2)#1-Sr(1)-O(2)	111.53(6)
O(2)#2-Sr(1)-O(2)	160.90(6)	O(2)#1-Sr(1)-O(2)	160.90(6)
O(2)#2-Sr(1)-O(2)	111.53(6)	O(2)-Sr(1)-O(2)	70.42(6)
O(2)#1-Sr(1)-O(1)	117.65(5)	O(2)#2-Sr(1)-O(1)	76.52(5)
O(2)-Sr(1)-O(1)	114.54(4)	O(2)-Sr(1)-O(1)	49.44(4)
O(2)#1-Sr(1)-O(1)	76.52(5)	O(2)#2-Sr(1)-O(1)	117.65(5)
O(2)-Sr(1)-O(1)	49.44(4)	O(2)-Sr(1)-O(1)	114.53(4)
O(1)-Sr(1)-O(1)	163.46(6)	O(2)#1-Sr(1)-N(1)	85.47(5)
O(2)#2-Sr(1)-N(1)	126.32(5)	O(2)-Sr(1)-N(1)	72.77(5)
O(2)-Sr(1)-N(1)	76.93(5)	O(1)-Sr(1)-N(1)	71.03(5)
O(1)-Sr(1)-N(1)	103.48(5)	O(2)#1-Sr(1)-N(1)	126.32(5)
O(2)#2-Sr(1)-N(1)	85.47(5)	O(2)-Sr(1)-N(1)	76.93(5)
O(2)-Sr(1)-N(1)	72.77(5)	O(1)-Sr(1)-N(1)	103.48(5)
O(1)-Sr(1)-N(1)	71.03(5)	N(1)-Sr(1)-N(1)	142.71(8)

Symmetry codes: for **1**: #1: x-1/2, -y+1/2, z-1/2; #2: x-1/2, y+1/2, z; #3: x, y+1, z. for **2**: x, -y, z+1/2; -x+1/2, y, z+1/2.

Table S3 Hydrogen bond distances (Å) and bond angles (°) for **1** and **2**

D-H···A	d(D-H)	d(H…A)	d(D…A)	∠(DHA)
1				
OW(1)-HW(1A)…O(4)	0.85	2.29	2.939(6)	133
OW(1)-HW(1A)…O(1)#1	0.85	2.57	3.106(7)	122
OW(1)-HW(1B)…O(2)#2	0.85	2.12	2.923(7)	158
C(3)-H(3A)…OW(1)#3	0.93	2.45	3.053(8)	122
C(5)-H(5A)…OW(1)#4	0.93	2.44	3.367(6)	173
C(6)-H(6A)…O(4)#5	0.93	2.43	3.161(6)	135
2				
C(11)-H(7A)…O(1)#1	0.93	2.51	3.094(2)	121

Symmetry codes: for **1**: #1: x, -y, z-1/2; #2: -x+1/2, y-1/2, -z-1/2; #3: x, -y-1, z+1/2; #4: -x, y, -z-1/2; #5: x-1/2, y+1/2, z. for **2**: #1: x, -y, z-1/2.

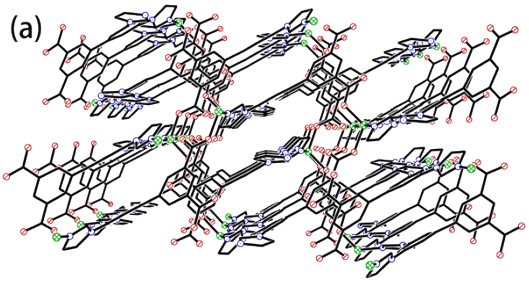

Fig. S1 The 3D network of **1** along b axis.

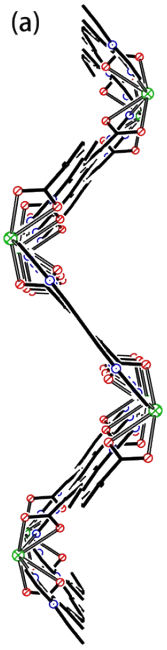

Fig. S2 (a) The zigzag chain along b axis.

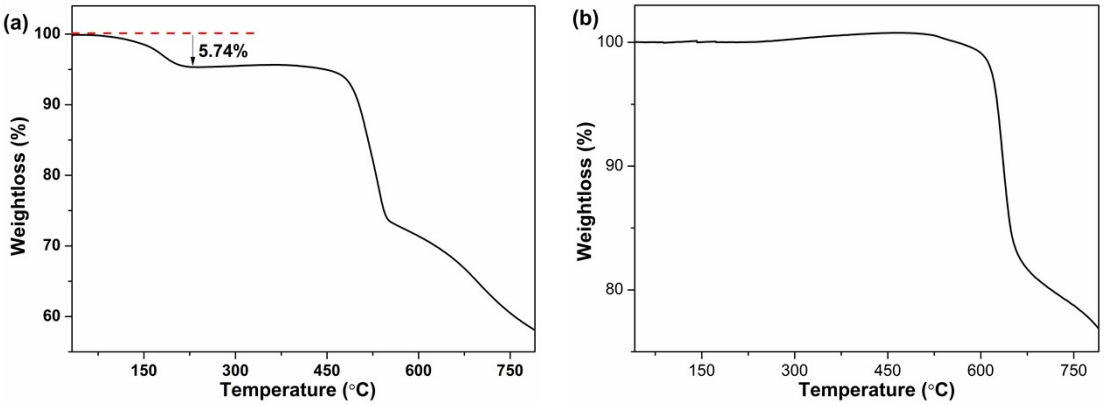

Fig. S3 The thermal analysis curve of compound **1** (a) and **2** (b).

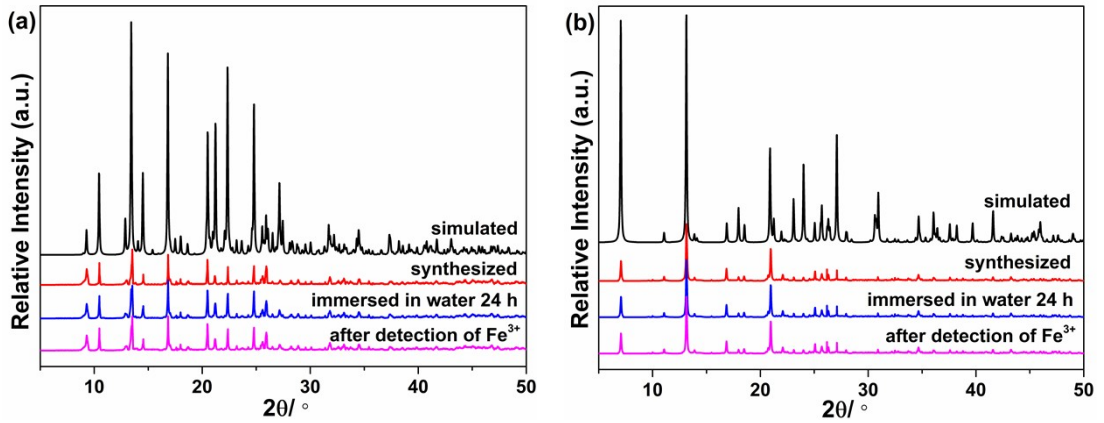

Fig. S4 PXRD pattern of compound **1** (a) and **2** (b), the immersed sample and the detection of Fe^{3+}.

Section 3 Detection of Fe^{3+}

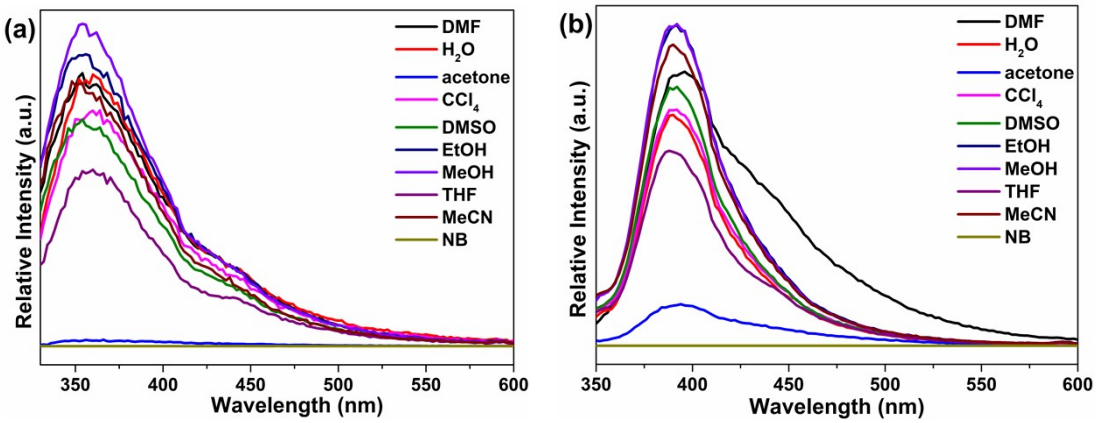

Fig. S5 Luminescent spectra of **1** (a) (λ_{ex}: 291 nm) and **2** (b) (λ_{ex}: 326 nm) in different solvents (Condition: 5 mg **1**, 3 mL solvent).

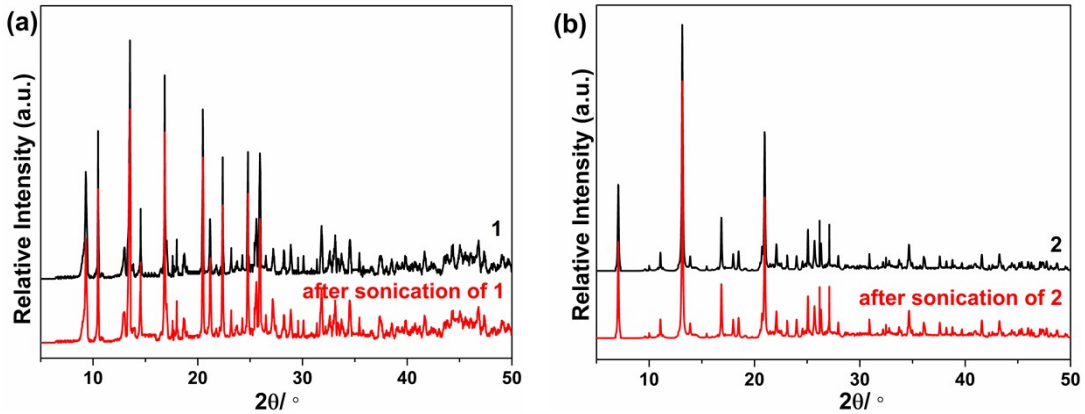

Fig. S6 PXRD pattern of compounds **1** (a) and **2** (b) before and after sonication in water.

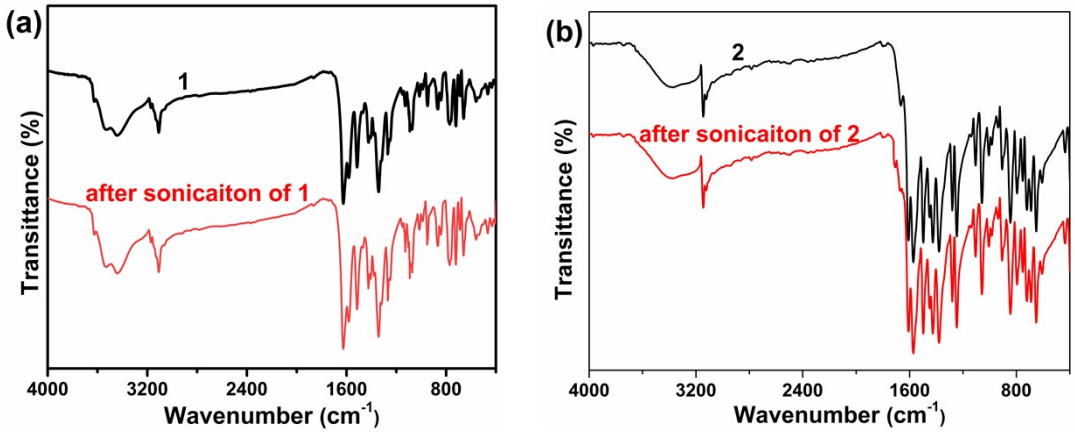

Fig. S7 IR spectra of compounds **1** (a) and **2** (b) before and after sonication in water.

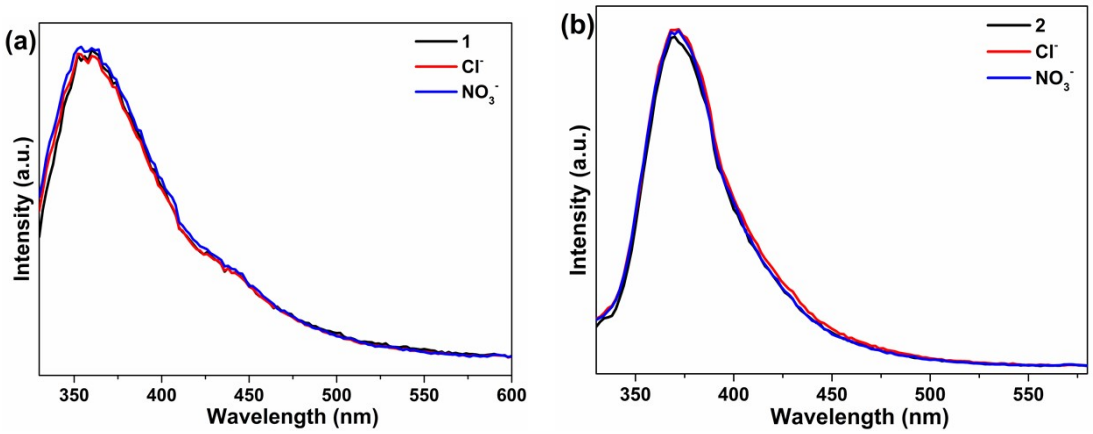

Fig. S8 The emission spectra of **1** (a) and **2** (b) immersed in water solution of NaCl and $NaNO_3$, respectively (Condition: 5 mg **1** (**2**), 3 mL H_2O and 0.02 mmol Na^+ ion).

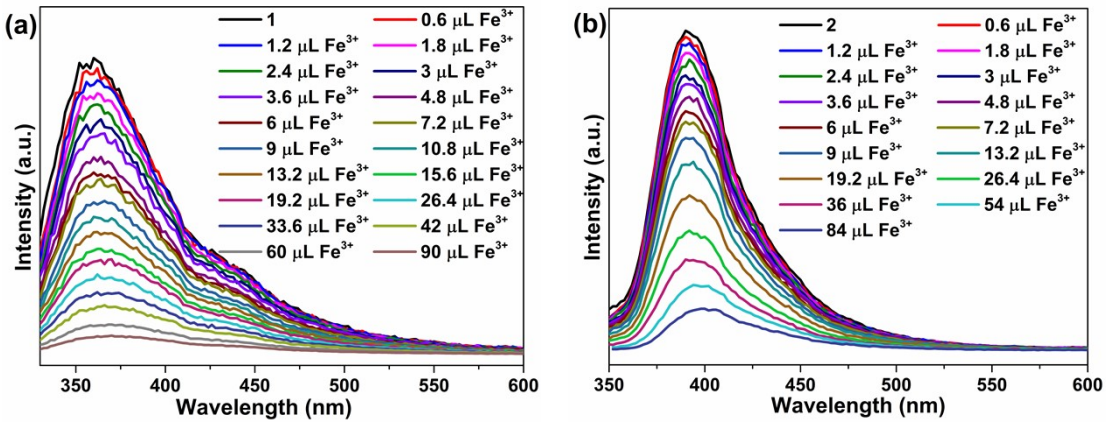

Fig. S9 Fluorescent spectra of **1** (a) and **2** (b) suspension (1.67 mg/mL) upon incremental addition of Fe^{3+} (0.01 M).

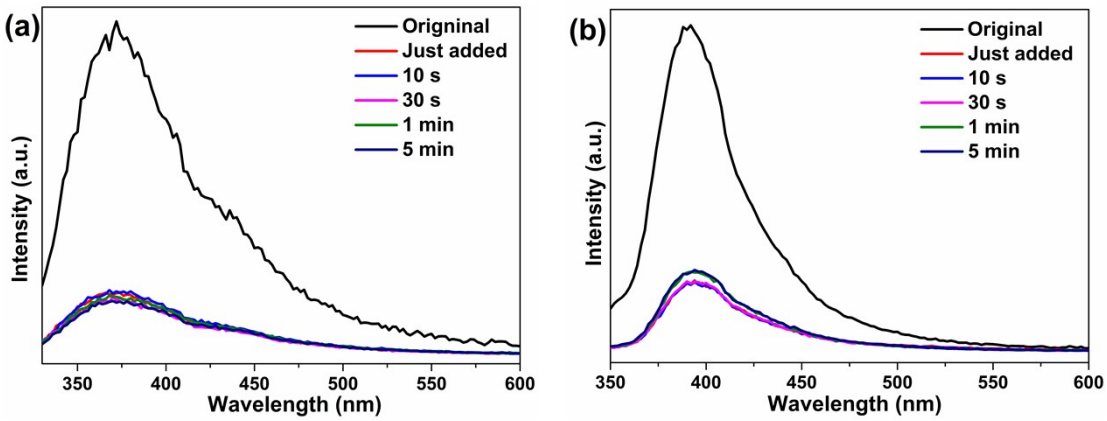

Fig. S10 Time-dependent fluorescent quenching detections of **1** (a) and **2** (b) for Fe^{3+}.

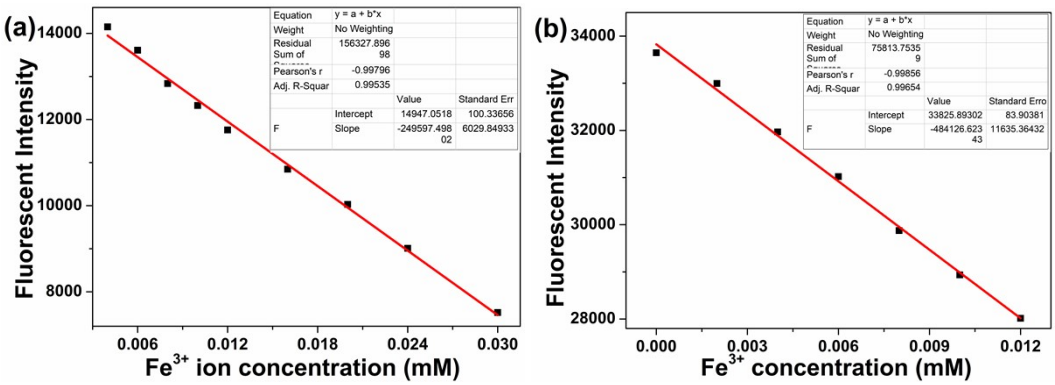

Fig. S11 Linear curve of fluorescent intensity of **1** (a) and **2** (b) suspension upon incremental addition of Fe^{3+}

Table S4 Standard deviation calculation

	Fluorescent intensity ($\times 10^4$)
Compound **1**	
Test 1	1.613
Test 2	1.626
Test 3	1.621
Continue	
Test 4	1.616
Test 5	1.624
Standard deviation (σ)	0.0054
Compound **2**	
Test 1	3.412
Test 2	3.422
Test 3	3.406
Test 4	3.426
Test 5	3.430
Standard deviation (σ)	0.0099

Table S5 Detection limit calculation for Fe^{3+}

Compounds	
1	
Slope (k)	2.50×10^5 mM^{-1}
Detection limit (3σ/k)	6.48×10^{-4} mM
2	
Slope (k)	4.84×10^5 mM^{-1}
Detection limit (3σ/k)	6.14×10^{-4} mM

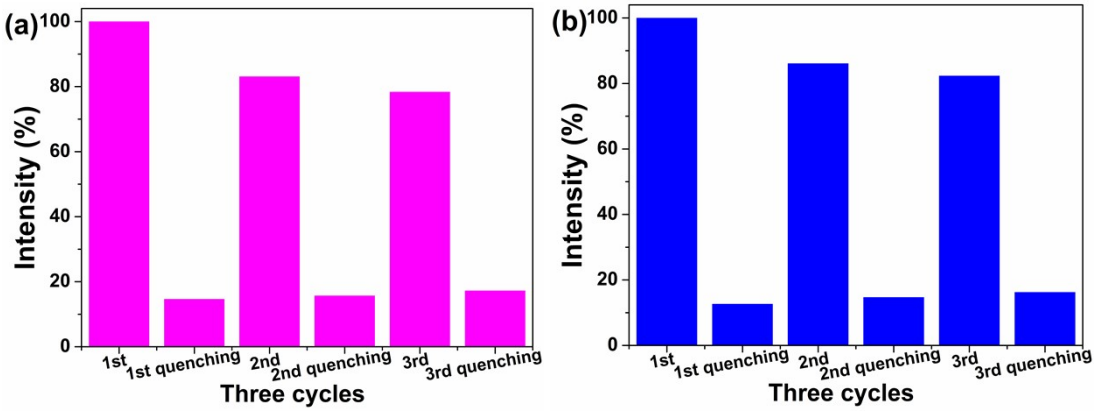

Fig. S12 Three quenching cycles of **1** (a) and **2** (b) suspension after addition of Fe^{3+}.

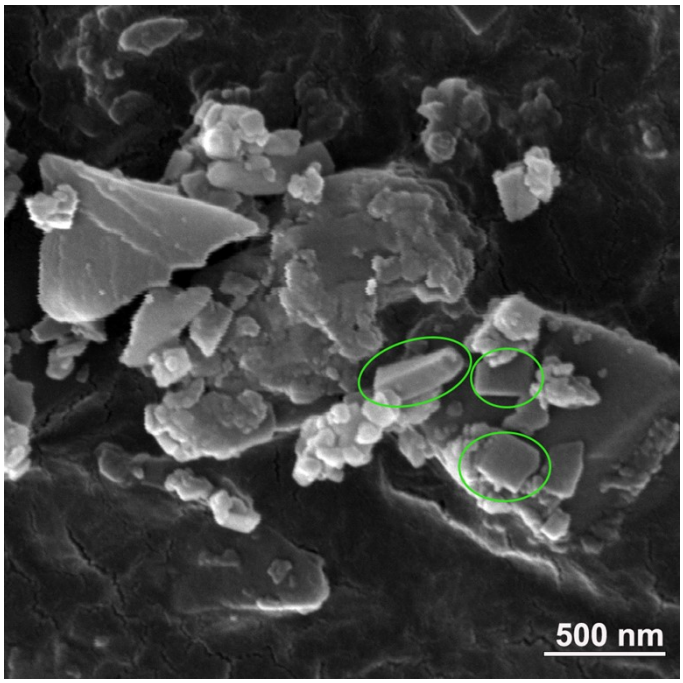

Fig. S13 SEM image of compound **1** after Fe^{3+} immersion.

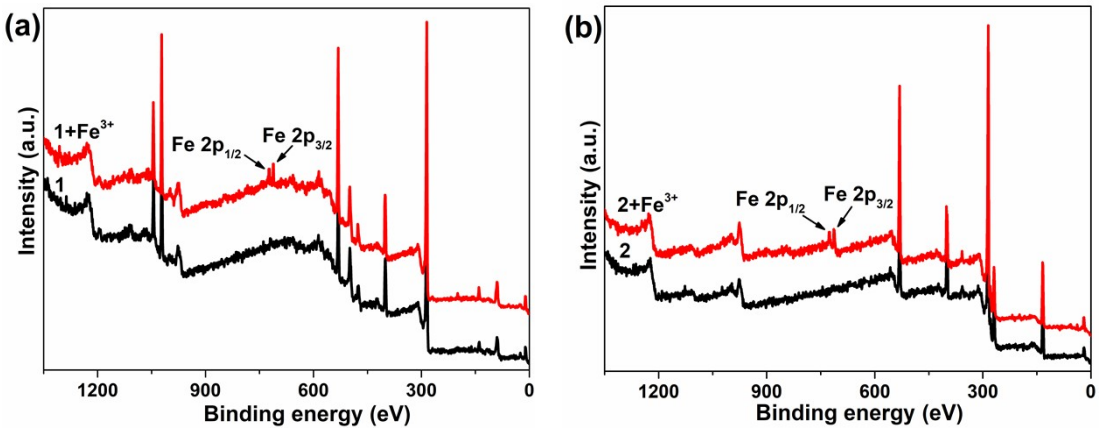

Fig. S14 XPS for compound **1** and Fe^{3+} incorporating **1** (a), **2** and Fe^{3+} incorporating **2** (b).

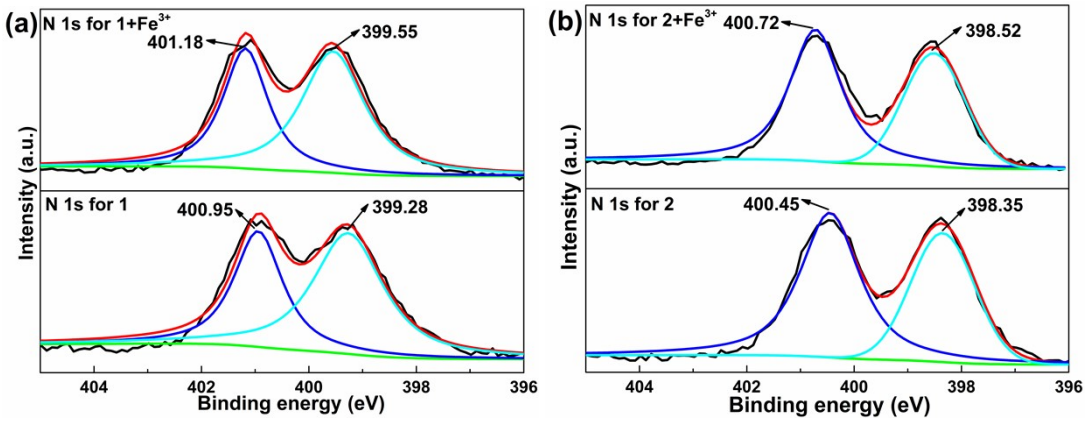

Fig. S15 XPS survey of N 1s of compounds **1** (a) and **2** (b) before and after binding with Fe^{3+}.

Table S6 The comparison of XPS peak-peak displacement values in 1 and 2

	1		**2**	
	$\Delta E_{C=O}$	ΔE_{C-O}	$\Delta E_{C=O}$	ΔE_{C-O}
O 1s	0.21	0.45	0.06	0.01
	ΔE_{C-N}	ΔE_{N-Zn}	ΔE_{C-N}	ΔE_{N-Sr}
N 1s	0.27	0.77	0.17	0.27

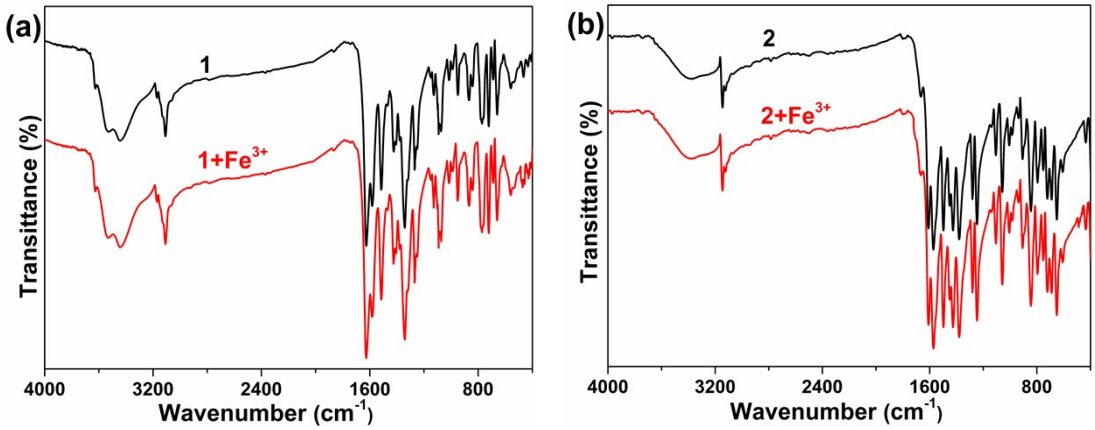

Fig. S16 (a) FT-IR spectra for compound **1** and Fe^{3+} incorporated **1**; (b) FT-IR spectra for compound **2** and Fe^{3+} incorporated **2**.

Reference

(S1) Q. Dong, K. Ge, M. Zhang, H. Wang and J. Duan, Rotation configuration control of the sp^2 bond inthe diimidazole-dicarboxylate linker for the isomerism of porous coordination polymers, *Dalton Trans.*, 2022, **51**, 12232-12239.